Four-Band Hamiltonian for fast calculations in intermediate-band solar cells

Antonio Luque, Aleksandr Panchak, Alexey Vlasov, Antonio Martí, Viacheslav Andreev

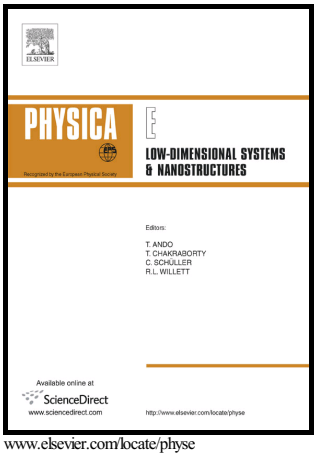

www.elsevier.com/locate/physe

PII: S1386-9477(15)30248-4
DOI: http://dx.doi.org/10.1016/j.physe.2015.10.019
Reference: PHYSE12166

To appear in: *Physica E: Low-dimensional Systems and Nanostructures*

Received date: 25 June 2015
Revised date: 24 September 2015
Accepted date: 16 October 2015

Cite this article as: Antonio Luque, Aleksandr Panchak, Alexey Vlasov, Antonio Martí and Viacheslav Andreev, Four-Band Hamiltonian for fast calculations in intermediate-band solar cells, *Physica E: Low-dimensional Systems and Nanostructures,* http://dx.doi.org/10.1016/j.physe.2015.10.019

Four-Band Hamiltonian for fast calculations in intermediate-band solar cells

Antonio Luque[1,2], Aleksandr Panchak[1], Alexey Vlasov[1], Antonio Martí[2] and Viacheslav Andreev[1]

1. Ioffe Physical Technical Institute, St. Petersburg, Russia
2. Polytechnic University of Madrid, Madrid, Spain

Corresponding Author Antonio Luque

e-mail address a.luque@upm.es

Key Words: Photovoltaics, Quantum Calculations, Photon Absorption, Quantum Efficiency, k·p Metods

The 8-dimensional Luttinger-Kohn-Pikus-Bir Hamiltonian matrix may be made up of four 4-dimensional blocks. A 4-band Hamiltonian is presented, obtained from making the non-diagonal blocks zero. The parameters of the new Hamiltonian are adjusted to fit the calculated effective masses and strained QD bandgap with the measured ones. The 4-dimensional Hamiltonian thus obtained agrees well with measured quantum efficiency of a quantum dot intermediate band solar cell and the full absorption spectrum can be calculated in about two hours using Mathematica© and a notebook. This is a hundred times faster than with the commonly-used 8-band Hamiltonian and is considered suitable for helping design engineers in the development of nanostructured solar cells.

1 Introduction

The use of an intermediate band (IB), that is, a band within the energy gap of a semiconductor, can raise the detailed balance efficiency limit [1] of a solar cell from 41% to 63%. [2] This IB serves as a stepping stone permitting two low-energy photons to generate an electron-hole pair in the valence (VB) and conduction (CB) bands of the semiconductor. The voltage may be maintained approximately if the IB has a quasi Fermi level (or electrochemical potential) different from that of the CB and the VB. Thus, a higher efficiency may be achieved.

One way of producing an IB is by forming quantum dots (QDs) in a host semiconductor,[3] e.g. QDs of InAs in a GaAs host material. The InAs QDs produce potential wells in the GaAs CB; the wells confine the electrons with energies which are within the GaAs bandgap; these energy levels may act as an IB. Other material combinations may also behave like the InAs/GaAs.

Despite the concept's promise, only on very seldom occasions have efficiencies greater than the cell without QDs been achieved [4] and even then, merely marginally. The main reason is the

weak absorption of the photons by the QDs. This absorption can be modeled using *ab initio* [5] or $\boldsymbol{k \cdot p}$ [6] calculations. In both cases the calculation resources are huge. The so called Empiric $\boldsymbol{k \cdot p}$ (EKP) Hamiltonian has been developed [7, 8] to permit a much faster calculation, feasible on a laptop. This may greatly aid the device scientist in obtaining feedback from calculations in the task of improving IB solar cells. It is based on building a Hamiltonian whose eigenvalues are the experimental $E(\boldsymbol{k})$ dispersion functions.

However, the well-established method for studying the quantum characteristics of the nanostructure materials with a zincblende structure (those currently providing the greatest efficiency) , including the absorption coefficients, is the use of the 8-band Luttinger Kohn (LK) [9, 10] Hamiltonian modified by Pikus and Bir (PB) [11, 12] to account for the strain in the lattice. This is a variety of the $\boldsymbol{k \cdot p}$ methods introduced by Dresselhaus, Kip and Kittel [13] and extensively developed by Kane.[14, 15]. It has been found [16] that the LKPB Hamiltonian is about 100 times more time consuming than the EKP Hamiltonian for typical problem sizes and parameters

The most important reason for this time-consuming feature is that the LKPB Hamiltonian uses eight bands in the problems associated with photon absorption for solar cells in zincblende semiconductors. In this article we propose a four-band Hamiltonian derived from the LKPB one and we will see that the time-consumption is close to that of the EKP Hamiltonian and therefore almost 100 times faster than the 8-band LKPB Hamiltonian.

Among the approximations that we adopt for simplicity is the QD shape, which is considered a squat parallelepiped or box instead of the squat truncated quadrangular pyramid that dictates the theory. [17] Other authors have used different shapes such as full pyramids,[18, 19] lenses[5] or, as we do, parallelepipeds.[7, 20-22]

The other approximation is the widely used concept of constant band offset, which considers the confining potential introduced by the QD as constant in all its volume, and zero outside it. We will describe the theoretical implications of this approximation.

Besides this Introduction, Section 2 contains the theoretical background where the basic aspects of the LKPB Hamiltonian are explained, in a big extent with the purpose of fixing the paper's nomenclature; it also explains the strain model that produces constant offsets and which is used in this paper for simplicity. Section 3 introduces the concepts in which the 4-band Hamiltonian is based. Section 4 presents results of this Hamiltonian concerning the energy spectrum, eigenstates and absorption coefficients, always in comparison with the EKP Hamiltonian and the 8-band LKPB Hamiltonian; the reasonable agreement achieved with the measured data constitute the main justification of this method. Section 5 comprises an estimate of the calculation time of the 4-band Hamiltonian as compared to that of the 8 band. Finally a conclusions Section 6 is added. The paper also contains an Appendix in which the formulas for calculating the LKPB Hamiltonian are described. An on-line Supplementary Data file accompanies the paper and includes Section 1, on the choice of parameters, Section 2, on the determination of the strain function, Section 3, on the strained material fitting of the effective masses and finally, Section 4 in which some of the properties of the Fourier transforms are set out.

2 Theoretical Background

k·p methods are based on developing a one-electron Hamiltonian into an orthonormal basis $|0,v,\boldsymbol{k}\rangle = |0,v\rangle \exp(i\boldsymbol{k}\cdot\boldsymbol{r})/\sqrt{\Omega}$ where $|0,v\rangle$ is a the Γ-point Bloch function (GBF), which has the periodicity of the lattice, v is the band index, $\boldsymbol{k}$ is an arbitrary wavevector of the first Brillouin zone and Ω is the volume of calculation (in this paper, a cube of 60×60×60 nm^3), which must be large with respect to the nanostructure studied here (a box of 16×16×6 nm^3). The 0 index refers to the Γ point ($\boldsymbol{k}$=0). We call this basis the standard basis. This standard basis is usually limited to a small number, n_B, of bands of interest. The matrix elements relating basis vectors of different $\boldsymbol{k}$ are automatically zero, so that the Hamiltonian is represented as a matrix of dimension n_B whose elements are functions of $\boldsymbol{k}$. The matrix usually undergoes the process known as renormalization [23] to account for the neglected bands.

For zincblende semiconductors, it is very common to use the conduction band (*cb*), and three valence bands (VBs): the heavy hole (*hh*) the light hole (*lh*) and the spilt off (*so*) bands. Disregarding the spin for the moment, the zincblende lattice belongs to the T_d symmetry group. The *cb* GBF is often called $|S\rangle$ and has spherical symmetry (it is an *s*-function). At $\boldsymbol{k}$=0, the three VBs degenerate and the eigenfunctions are linear combinations of three GBFs called $|X\rangle$, $|Y\rangle$ and $|Z\rangle$ with the symmetry of *x*, *y* and *z* (see, e.g. Datta[23]) respectively (they are *p*-functions). However each of these functions may be considered with spin up or down and denoted as $|S\uparrow\rangle$… $|Y\downarrow\rangle$ etc.

In the EKP Hamiltonian we neglect the spin and use $|S\rangle$, $|X\rangle$, $|Y\rangle$ and $|Z\rangle$ to form the standard basis. This leads to a 4-band Hamiltonian. Furthermore, we use a simple Hamiltonian (H_0) that neglects the important spin-orbit coupling and any strain effect. The eigenvalues of a ***k·p*** Hamiltonian are the $E(\boldsymbol{k})$ dispersion functions, whose details can be seen in e.g., Datta.[23] These dispersion functions are replaced in the EKP Hamiltonian by parabolic experimental ones, characterized by the band edges and effective masses, but the eigenvectors of (H_0) are retained. See [8, 20] for details.

In contrast, the spin is taken into account in the LK Hamiltonian and when the origin of energy is set at the VB top, eigenvalues are E_g, E_g, 0, 0, 0, 0, $-\Delta$, $-\Delta$, where E_g and $-\Delta$ are experimental data characteristic of the material. The eigenvectors are linear combinations of the states $|S\uparrow\rangle$… $|Y\downarrow\rangle$ etc. and in this paper they are labeled as $|cb+\rangle$, $|hh+\rangle$, $|lh+\rangle$, $|so+\rangle$, $|cb-\rangle$, $|hh-\rangle$, $|lh-\rangle$, $|so-\rangle$. For details see reference [23].

As the number of eigenvalues is 8, the LK Hamiltonian is represented by an 8-dimension (8D) matrix. If the eigenvectors are ordered as indicated above, the 8D matrix may be divided into four blocks.[19]

$$(H) = \begin{pmatrix} (H_{uu}) & (H_{ul}) \\ (H_{lu}) & (H_{ll}) \end{pmatrix} \tag{1}$$

The interesting aspect of this block separation is that is $(H_{lu}) = (H_{ul}^{+})$ (hermitical conjugate) and $(H_{ll}) = (H_{uu}^{*})$ (complex conjugate); therefore, only two of the four matrices have to be determined.

Each one of the block matrices may be considered the sum of a kinetic matrix (the LK part), which applies to non-strained materials, and a strained material matrix (the PB part). Auxiliary functions are defined to write the matrix elements, and are presented in the Appendix. For different materials they depend of a set of parameters that can be found in the literature.[24]

All the LK matrix elements are functions of $\boldsymbol{k}$; the PB matrix elements depend on elements of the strain tensor. The strain tensor elements are multiplied by material-dependant factors which relate them to the electronic energy that these displacements produce. Many elements of the PB matrix elements are constant with respect to $\boldsymbol{k}$. However some of them are function of it (see the Appendix).

The $E(\boldsymbol{k})$ dispersion functions, which are the eigenvalues of (H) calculated for different values of $\boldsymbol{k}$, are doubly degenerated for all the values of $\boldsymbol{k}$. The degeneration refers to the spin, for instance, the ($lh+$) and the ($lh-$) bands degenerate. In Figure 1 we present the dispersion functions for the (H) and (H_{uu}) matrices of the Appendix calculated using the parameters selected in the Supplemental Supporting Material of this paper (Table S 2, "Unstrained 8B parameters" column). The reason for also plotting the dispersion functions of (H_{uu}) will become clear later.

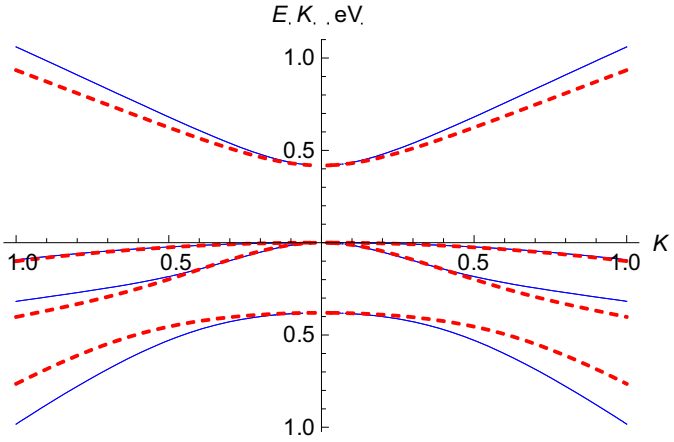

Figure 1. Dispersion curves of (H) and (H_{uu}) with the chosen parameters in the (1,1,1) direction. Solid line (blue) for the 8B (H), dashed line (red) for the 4B (H_{uu}). The set of curves from up to down correspond to the *cb*, the *hh* the *lh* and the *so* bands. $K=kd$ with d an arbitrary normalizing length that in this paper is taken as 1 nm.

For unstrained material, all the PB matrix elements are zero. Furthermore, for $\boldsymbol{k}=0$ all the non-diagonal elements of the LKPB matrix are also zero and the diagonal elements of (H_{uu}) or of (H_{ll}) are E_g, 0,0,$-\Delta$. For the matrix (H) they are the same, double degenerate.

The parameters selected in the Supplemental Supporting Material give an excellent agreement with the experimental band positions and with the effective masses (see Böer [25] for details on the experimental methods) of the *cb*, *hh* and *lh* bands, as shown in Table 1 ("Unstrained 8B parameters" column); the *so* band effective mass is not well reproduced but the *so* electrons do not contribute to the sub-bandgap absorption because their energy is too low (they absorb photons of energy above the bandgap); therefore we do not take its value into account. The effective masses present the isotropy that is expected for the Γ point.

Table 1. Band edges and effective masses with the parameters obtained in the Supplemental Supporting Material and experimental values.[26, 27]

Band edges and relative effective mass	Unstrained 8B parameters	Experi-mental un-strained [26]	4B-strained & fitted	Experi-mental strained [27]
E_c (eV)	0.418	0.418	0.737	0.737
E_{vhh} (eV)	0	0	-0.032	0
E_{vlh} (eV)	0	0	-0.031	0

E_{vso} (eV)		-0.38		-0.38		-0.412		-0.212
Direction	(1,1,1)	(1,0,0)	(0,0,1)	Any	(1,1,1)	(1,0,0)	(0,0,1)	Any
m_{cb}/m_0	0.023	0.023	0.023	0.023	0.0294	0.038	0.020	0.0294
m_{hh}/m_0	-0.410	-0.410	-0.410	-0.41	-0.333	-0.337	-0.301	-0.333
m_{lh}/m_0	-0.026	-0.026	-0.026	-0.026	-0.027	-0.030	-0.024	-0.027
m_{so}/m_0	-0.077	-0.077	-0.077	-0.16	-0.123	-0.285	-0.058	-0.076

The introduction of a nanostructure into a host of a different lattice parameter leads to a deformation of both materials. They significantly affect the electronic variables. Energy eigenvalues and eigenstates are modified. The deformations vary with the position and consequently, so do the band edges, affecting the offset potentials that, notwithstanding, in many cases are taken as square for simplicity. These squared potentials are only possible if very simple deformation tensors are used. Consequently, we assume that the host material is not deformed and that the QD material tends to adopt the lattice parameters of the host material, becoming in pure compression. With these assumptions the strain tensor terms are,

$$\varepsilon_{xx} = \varepsilon_{yy} = \varepsilon_{zz} = \chi_s \left(\frac{l_c(\mathrm{InAs})}{l_c(\mathrm{GaAs})} - 1 \right)$$
$$\varepsilon_{xy} = \varepsilon_{yz} = \varepsilon_{zx} = \varepsilon_{yx} = \varepsilon_{zy} = \varepsilon_{xz} = 0 \qquad (2)$$

where χ_s is calculated in the Supplementary Data file to obtain the experimental bandgap [28] of the strained material to fit the bandgap when the QDs are inserted.; its value is χ_s=0.239. Details of the calculation of the strain tensor terms are in reference. [16]

In reality, the host lattice constant is also modified and strong shear stresses appear on the edges. Not all the potential is squared; it has peaks on the edges and extends outside the QD. However, real potential distributions [18, 29] approach the squared potential reasonably well. For the sake of comparison with the EKP Hamiltonian and for simplicity we have ignored these complexities and adopted square potentials.

3 The 4-band LKPB Hamiltonian

The basic idea for proposing a 4-band LKPB Hamiltonian is to use the (H_{uu}) sub-matrix of Eq. (1) only. As discussed later, this would be totally correct if the non-diagonal blocks of (H) were zero or negligible (remember that they are hermitical conjugate, so that if one is zero the other is zero too). That is,

$$(H_{4B}) = \begin{pmatrix} (H_{uu}) & (0) \\ (0) & (H_{ll}) \end{pmatrix} \qquad (3)$$

In this case (H_{ll}) is the complex conjugate of (H_{uu}) and has the same (real) eigenvalues thus leading to the degenerate dispersion functions which are general to the matrix (H).

The differences found in Figure 1 between the dispersion functions of (H) and (H_{uu}) reflect the fact that the off-diagonal blocks are not zero. The basic idea in this work is to fit the parameters to be used in the Hamiltonian calculation procedure in such a way that the effective masses are reproduced by the (H_{uu}) eigenfunctions. Details of the fitting procedure are in the Supplementary Data and the parameters used are in Table S 2 ("4B strained fitting" column) of that document. The bands' positions and the calculated effective masses appear in Table 1 ("4B-

strained & fitted" column). The coincidence of the calculated and experimental effective masses is perfect in the (111) direction, in which the fitting is made, with the exception of m_{so} which is not of interest in this case. For the remaining the directions, the isotropy is reasonable. In practice we will use the experimental effective masses, when using this Hamiltonian, equal in all the directions.

4 Energy spectrum, states and absorption coefficients

4.1 The energy spectrum

The energy spectrum of the GaAs with the InAs QDs inserted may be obtained from the effective mass Schrödinger equations, which are

$$-\frac{\hbar^2}{2m_v^*}\nabla^2\Phi(\boldsymbol{r})+{}^vU(\boldsymbol{r})=E\Phi(\boldsymbol{r}) \tag{4}$$

The potential ${}^vU(\boldsymbol{r})$ is the v-band offset and m_v^* is the effective mass for band v. For the VBs the effective mass is negative; the offset pedestals are electron confining as are the wells in the CB. If this equation is changed of sign for the VBs, the energies become negative, that is, they must be counted from up to down, as is usual. Since the bound wavefunctions span mainly within the QD, the effective masses are those of their material, in this paper, InAs. An alternative is to use the Bastard boundary conditions,[30] involving QD and host effective masses. We have not used them because the differences are very small for the states of interest.

Since the band offset is considered constant and the effective mass is fitted to be the same as the experimental one, there is no difference between the results with the 4-band in this paper and the EKP Hamiltonians[7, 20]. The energy spectrum is exactly the same.

Eq. (4) can be solved by considering it as separable. In this case it involves the resolution of three simple 1-dimensional (1D) equations.[31] For 1D energies below the potential rim (above the pedestal base for the VBs) only certain values of the energy lead to bound solutions and can therefore be retained. These are even (cos) of odd (sin) harmonic solutions within the QW flanked by fading exponentials outside it. A quantum natural number may be established which denotes the solutions in increasing order of the 1D energy they corresponds to. For 1D-energy above the well rim, any energy value leads to a solution which is harmonic inside and outside the QW. This corresponds to extended states or electrons that travel rather freely.

3D solutions are the product of three 1D solutions, each for one x, y or z variable. They are denoted by three quantum numbers, corresponding to the three 1D solutions. The energy is the sum of the three 1D energies. If the three 1D energies are below the potential well rim (above the pedestal base) the 3D solutions are bound. Their energy is sometimes below the well rim (above the pedestal base) and therefore they are within the host-material bandgap. However their energy may be above the potential well (below the pedestal base), that is, within the CV (VB) of the host material. In other words, they are degenerate (have the same energy) with free electrons (holes). These are called virtual bound states and play an important role in the interband optical transitions, which are those that create electron-hole pairs.

The potential well (pedestal) is not exactly separable but it is a good approximation for the states within the host material bandgap and the virtual bound states close to the band edges; this has been thoroughly studied.[32] The multiband energy spectrum for the bound functions is

presented in Figure 2. In this spectrum the inaccuracies of the separable assumption are corrected.[32] In the figure, the CB well and the VB pedestals formed by the band offsets between the InAs QD material and the GaAs host are represented. The values of the offsets and the QD dimensions appear in the figure caption. The effective masses are in Table 1 ("Experimental strained" column).

This spectrum reproduces the number of levels obtained by photoluminescence [33, 34] or by photoreflectance spectroscopy.[35]

The three lower energy *cb* levels within the host material bandgap are the IB levels. They can be labeled as $|cb111\rangle$, $|cb121\rangle$, $|cb211\rangle$, $|cb221\rangle$ or as $|IB111\rangle$, etc. The states $|cb121\rangle$ and $|cb211\rangle$ are degenerate, as well as all those made through the permutation of the first two (x- and y-) quantum numbers. $|cb131\rangle$ is considered to be already in the CB and therefore in full thermal contact with it (the same electrochemical potential).

The *hh* states are very densely packed and therefore form a quasi continuum, in full thermal contact with the VB; actually they constitute a tail of it, although with a faint density of states, much smaller than that of the bulk semiconductor. The light holes, immersed in this tail, are also in thermal contact with the VB.

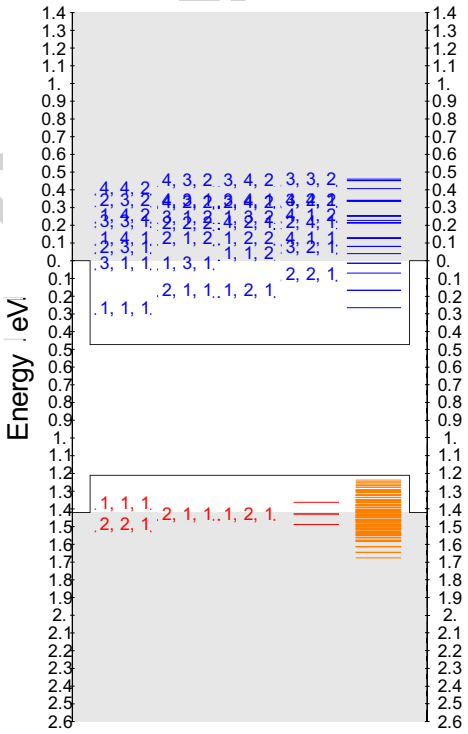

Figure 2. Bound eigenfunction spectrum for eigenfunctions in the *cb* (blue), the *hh* (orange) and the *lh* (red) bands. The quantum numbers are also shown except for the *hh* due to lack of space. The QD size is 6×16×16 nm^3. The CB and VB offsets are V_{CBO}=0.473 eV and V_{VBO}=0.210 eV respectively.

4.2 The envelope functions

In the ***k·p*** model any eigenfunction, irrespective of the number of bands n_B, is considered to be of the form

$$\Xi(\boldsymbol{r}) \cong \sum_{v} |0,v\rangle \Psi_v(\boldsymbol{r}) \tag{5}$$

where $|0,v\rangle$ are the GBF, $\Psi_v(\boldsymbol{r})$ are the so-called envelope functions and v is the band index. For this to be true, it is necessary for the envelope functions to vary negligibly within the unit cells of the crystal. The envelope functions can be obtained [7, 8, 23] as follows: (a) calculate the $\Phi(\boldsymbol{r})$ function of the effective mass Schrödinger equation, (b) obtain its discrete Fourier transform (DFT) $\phi_{\boldsymbol{k}}$, (c) multiply it by the complex conjugate of corresponding diagonalization matrix element $(D_{\boldsymbol{k}})^{*}_{i,j}$ and (d) obtain the inverse discrete Fourier transform (IDFT). These four rules are further explained below.

The function $\Phi(\boldsymbol{r})$ must be calculated for the band and quantum numbers we want $\Xi(\boldsymbol{r})$ to belong to. The DFT is actually the development of $\Phi(\boldsymbol{r})$ in plane waves $\exp(i\boldsymbol{k}\cdot\boldsymbol{r})/\sqrt{\Omega}$. It is calculated in a certain calculation cube that must extend beyond the region in which the bound function $\Phi(\boldsymbol{r})$ is significant. Note that we assume that the QDs are isolated and no lattice of QDs is formed; for the vertical coordinate this is fully justified because in the solar cells the spacing between QD layers is about 80 nm and approximately justified for the horizontal separation between QDs which is about 7 nm. The calculation cube is divided into a 3D array of $\boldsymbol{r}$-nodes (separated 1.5 nm between them in this paper) so that a 3D array of Φ values is obtained. A 3D array of $\boldsymbol{k}$ wavevectors is also used with a number of nodes equal to the calculation nodes. All the wavevectors in the nodes confer the periodicity of the calculation cube to the plane waves.

Each row of the diagonalization matrix ($D_{\boldsymbol{k}}$) is made up of the eigenvectors, once normalized to one. This is a unitary matrix that has the property of diagonalizing the Hamiltonian matrix ($H_{\boldsymbol{k}}$), that is, $({}^{d}H_{\boldsymbol{k}})=(D_{\boldsymbol{k}})(H_{\boldsymbol{k}})(D_{\boldsymbol{k}}{}^{+})$ is diagonal and the diagonal elements are the eigenvalues, or $E(\boldsymbol{k})$ dispersion functions, of ($H_{\boldsymbol{k}}$) which are approximately parabolic with the experimental effective masses after the fitting that has been made. The cross + represents the hermitical conjugation (transpose of the complex conjugation).

The element $(D_{\boldsymbol{k}})_{i,j}$ of this matrix must be chosen in such a way that the row index i represents the band ($cb+$, $hh-$…) were Φ is calculated, and the column index j represents the envelope $\Psi_v(\boldsymbol{r})$ we are calculating. All the envelopes in Eq. (5) are obtained by repeating the aforementioned procedure (a-d) for all the elements of a row i. Details of these calculations may be found in reference [20].

If the (H) Hamiltonian non-diagonal blocs $(H_{ul})=(H_{lu})=(0)$ then the eigenvectors corresponding to a spin + band have components only in the spin + terms (they are decoupled to the spin – terms) and similarly for the spin – band. Consequently ($D_{\boldsymbol{k}}$) is a matrix of diagonal blocks only. Through step (c) of the rule for obtaining the envolvents, for a eigenfunction of the ($cb+$) band, for example, only the spin + terms are non zero, that is, Eq. (5) becomes

$$\Xi^{(cv+)} = \Psi^{(cv+)}_{|cb+\rangle}|cb+\rangle + \Psi^{(cv+)}_{|hh+\rangle}|hh+\rangle + \Psi^{(cv+)}_{|lh+\rangle}|lh+\rangle + \Psi^{(cv+)}_{|so+\rangle}|so+\rangle \tag{6}$$

and similar expressions for other bands (the bands of spin "–" only have "–" components). Actually, it is like having used only the 4-band Hamiltonians (H_{uu}) or (H_{ll}).

The procedure indicated is the same as that used for the 4-band EKP Hamiltonian.[7, 20] In this case the spin sign is ignored. However, there is a difference: the GBFs are $|X\rangle$, $|Y\rangle$, $|Z\rangle$ and $|S\rangle$ instead of $|cb+\rangle$, $|hh+\rangle$…or $|cb-\rangle$, $|hh-\rangle$…etc. As we shall see, this difference is of no importance for the photon absorption calculations if Eq. (5) can be applied.

Statement viii of the Supplementary Data asserts that the discrete Fourier transform (DFT) $\phi_{\boldsymbol{k}}$ of $\Phi(\boldsymbol{r})$ is either real or pure imaginary. Statement ix asserts that if $f(\boldsymbol{k})$ is the 3D DFT of $F(\boldsymbol{r})$ the inverse DFT (IDFT) of $f(\boldsymbol{k})^*$ is $F(-\boldsymbol{r})^*$.

If the envolvents for a +band of Eq. (6) have been calculated, it is not necessary to calculate those of a –band. In effect, since $(H_{ll})=(H_{uu}^*)$ their eigenvectors are complex conjugate and the diagonalization matrices $(D_{ll})=(D_{uu}^*)$. According to rule (d) of the procedure to obtain the envelope functions, $(D_{uu,\boldsymbol{k}})_{i,j}\phi_{\boldsymbol{k}}$ is the DFT of any of the + envelopes of Eq. (6),with simplified notation, $\Psi^+(\boldsymbol{r})$. The IDFT of $(D_{uu,\boldsymbol{k}})_{i,j}^*\phi_{\boldsymbol{k}}$ is $\Psi^-(-\boldsymbol{r})^*$. According to statement viii, we can consider the two cases of $\phi_{\boldsymbol{k}}$ as real or pure imaginary and in agreement with statement ix we can assert that:

I. When $\phi_{\boldsymbol{k}}$ is real, $\Psi^-(\boldsymbol{r})=\Psi^+(-\boldsymbol{r})^*$
II. When $\phi_{\boldsymbol{k}}$ is pure imaginary, $\Psi^-(\boldsymbol{r})=-\Psi^+(-\boldsymbol{r})^*$

In summary, the –band envelopes are the origin-reflected complex conjugate of those in Eq. (6), changed of sign if the number of odd 1D functions in the separation of variables solution of Φ) is odd (statement viii). In all cases, $\left|\Psi^{(cv+)}_{|cb+\rangle}(\boldsymbol{r})\right|=\left|\Psi^{(cv-)}_{|cb-\rangle}(-\boldsymbol{r})\right|$, and the same for other envelopes.

Furthermore, integral relationships of the type $\left\langle\Psi^{(+)}_{|cb+\rangle}\middle|\Psi^{(+)}_{|cb+\rangle}\right\rangle=\left\langle\Psi^{(-)}_{|cb-\rangle}\middle|\Psi^{(-)}_{|cb-\rangle}\right\rangle$ (the integral extended to all the space is invariant with the reflection), representing the projection of the wavefunction in the GBFs |cb+⟩ and |cb–⟩ respectively, are also fulfilled.

4.3 The absorption coefficients

The photon absorption coefficient between bound states is given by the expression $\alpha_{\Xi\to\Xi'}$ which achieves its maximum value when the Ξ-state is totally full of electrons and the Ξ'-state is totally empty. For partially filled states, the fraction of full initial states and the fraction of empty final states act as factors. The maximum absorption is,[7, 8]

$$\alpha^{max}_{\Xi\to\Xi'}=\alpha'_{\Xi\to\Xi'}E\delta(E_{line}-E);\quad \text{with}\quad \alpha'_{\Xi\to\Xi'}=\frac{2\pi^2q^2}{n_{ref}ch\varepsilon_0}\frac{\left|\left\langle\Xi\middle|\boldsymbol{r}\cdot\boldsymbol{\varepsilon}\middle|\Xi'\right\rangle\right|^2}{4ab}F_sN_l \tag{7}$$

where $\alpha'_{\Xi\to\Xi'}$ is used for convenience. It contains the electron charge q, the semiconductor index of refraction n_{ref} the speed of light c, the Planck constant h and the free-space permittivity ε_0. It also contains the QD base surface ab, the QD surface coverage fraction F_s by one layer of QDs and the number of layers N_l per unit of length. It finally contains the dipole element of matrix $\left\langle\Xi\middle|\boldsymbol{r}\cdot\boldsymbol{\varepsilon}\middle|\Xi'\right\rangle$ where $\boldsymbol{\varepsilon}$ is the photon polarization vector. The Dirac delta is usually substituted by a Gaussian (to account for technology variations) whose standard deviation is 0.025 eV in this article.

If the envelope functions do not vary significantly within a crystal unit cell, the matrix element may be written as a function of the envelopes only,[7, 8]

$$\left\langle\Xi\middle|\boldsymbol{\varepsilon}\cdot\boldsymbol{r}\middle|\Xi'\right\rangle\cong\sum_v\left\langle\Psi_v\middle|\boldsymbol{\varepsilon}\cdot\boldsymbol{r}\middle|\Psi'_v\right\rangle \tag{8}$$

For instance, for a transition between an initial state of the (*hh*+) band and a final state of the (cb+) band, in the 4B approximation, taking into account that only four envolvents are non-zero, Eq. (8) becomes,

$$\left\langle \Xi^{(hh+)} \left| \boldsymbol{\varepsilon}\cdot\boldsymbol{r} \right| \Xi^{(cb+)} \right\rangle \cong \left\langle \Psi^{(hh+)}_{|cb+\rangle} \left| \boldsymbol{\varepsilon}\cdot\boldsymbol{r} \right| \Psi^{(cb+)}_{|cb+\rangle} \right\rangle + \left\langle \Psi^{(hh+)}_{|hh+\rangle} \left| \boldsymbol{\varepsilon}\cdot\boldsymbol{r} \right| \Psi^{(cb+)}_{|hh+\rangle} \right\rangle + \left\langle \Psi^{(hh+)}_{|lh+\rangle} \left| \boldsymbol{\varepsilon}\cdot\boldsymbol{r} \right| \Psi^{(cb+)}_{|lh+\rangle} \right\rangle + \left\langle \Psi^{(hh+)}_{|so+\rangle} \left| \boldsymbol{\varepsilon}\cdot\boldsymbol{r} \right| \Psi^{(cb+)}_{|so+\rangle} \right\rangle \quad (9)$$

Let us now consider the (−)→(−) transitions; the expression is similar, if we replace the signs + in the indices by the sign −. In the case of (+)→(−) or (−)→(+) transitions, the matrix elements are zero because in the eight terms that might appear, one of the envolvents is zero. Furthermore, for the (−)→(−) transitions, all the envelopes are the reflections of the (+)→(+) transitions multiplied or not by −1, according to the summary assert viii of the Supplementary Data just presented, and by a minus sign resulting from $\boldsymbol{\varepsilon}\cdot\boldsymbol{r}$. However, the term $\left| \left\langle \Xi^{(hh+)} \left| \boldsymbol{\varepsilon}\cdot\boldsymbol{r} \right| \Xi^{(cb+)} \right\rangle \right|^2$, which is what actually appears in the absorption coefficient, is the same for the (hh+)→(cb+) and the (hh−)→(cb−) transitions. The same rule holds for other bands.

What has been said above about the 4B LKPB Hamiltonian is applicable to the EKP Hamiltonian. Taking into account the two spins of the |X⟩, |Y⟩, |Z⟩ and |S⟩ GBFs, its 8B Matrix contains two identical diagonal blocs, each one with the 4D EKP Hamiltonian.

In contrast, in the 8B LKPB Hamiltonian, the crossed spin transitions are not zero and each matrix element contains 8 terms that must be calculated.

In summary, only the absorptions between states of the same spin are not zero; their value is the same irrespective of the spin considered. In the absorption coefficients it is sufficient to calculate those of one given spin and to multiply the result by 2 to account for the other spin.

Rule (c) of the procedure to obtain envelopes can be modified for the calculation of absorption coefficients. The complex conjugation of $(D_{\boldsymbol{k}})^*_{i,j}$ is unnecessary. If it is not done we are calculating the absorption coefficients of the –bands, but, as proven, this gives the same result.

Figure 3 shows photon absorption coefficients calculated with the four-band (H_{uu}), To draw every curve the absorptions between every *hh* or *lh* (indicated by the two letters in the label) state and a *cb* state (indicated by the three digits) are added together. The unlabeled black curve is the sum of the absorptions from the VB to all the levels in the conduction band in the sub-bandgap range of energies. The *so* band is not calculated because it falls outside this range.

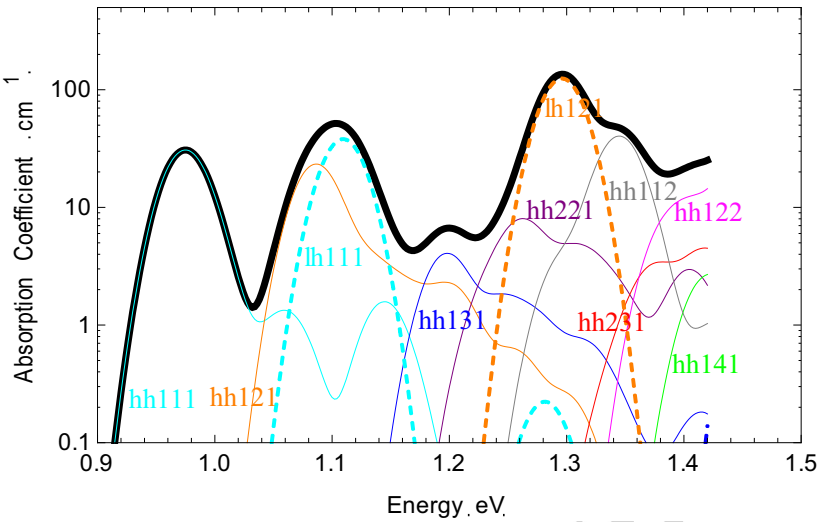

Figure 3. Sub-bandgap absorption calculated with the LKPB (H_{uu}) (thick black line) and contribution of the transitions from all the bound states in the *hh* and *lh* bands to the *cb* states (including the IB states). In the legends each curve is labeled with two letters for the initial states and the quantum numbers of the *cb* final state.

For these calculations it has been assumed that the VB states are all full of electrons and the *cb* states are empty. Size and potential offsets are those used for the energy spectrum calculations of Figure 2.

Figure 4 shows the internal quantum efficiency (IQE) calculated from the preceding absorption coefficients (red dashed curve) together with the measured one (green solid) and those calculated with the EKP Hamiltonian[20] (blue dot-dashed curve) and the 8-band LKPB (H)[16] (black dotted curve). It is assumed that all generated electron-hole pairs are collected at the solar cell terminals. It is also assumed that all the VB→IB absorptions are transported to the CB by thermal photons or phonons. All the IQEs calculated are within the order of magnitude of the real absorption, stressing the semi-quantitative nature of our approaches.

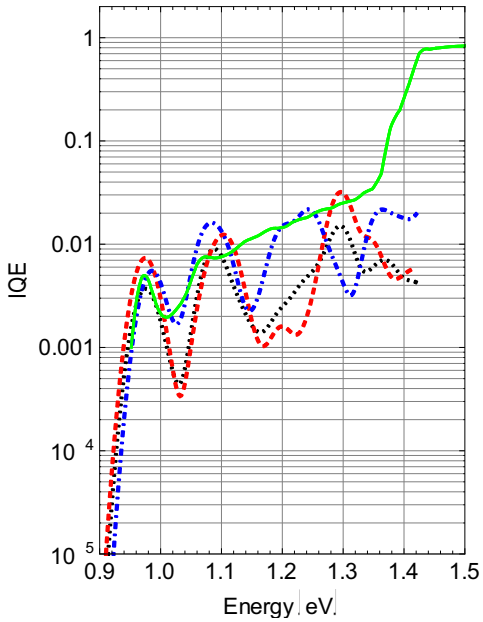

Figure 4. Measured Internal Quantum Efficiency (IQE) of the SOTA cells (green solid line) as compared with the EKPH calculation for 0.2 Givens rotation (blue, dot-dashed curve), the four band LKPB (H_{uu}) (red dashed curve) calculation and the eight band LKPB (black dotted curve) calculation. In all the calculations, the fundamental IB $|cb111\rangle$ state is assumed to be prefilled at 20% by doping.

The 8 band LKPB calculation is below the rest of the calculations including the experimental one. It seems surprising that this calculation, which, a priori, was deemed the most accurate, replicates the experimental data the worst. However, the approximations adopted as regards the

strain must not be forgotten. In addition, the EKP Hamiltonian has a fitting parameter. In the spin-orbit neglecting Hamiltonian the *hh* and the *so* eigenvalues are degenerate for all the $\boldsymbol{k}$s; therefore the eigenvectors may be validly adopted with one degree of freedom. A Givens rotation leaves the subspace spanned by *cb* and *lh* eigenvectors invariant and turn the axes of the other two subspace. The Givens rotation becomes a fitting parameter, so it is not surprising it can lead to a better fitting. This better fitting is at the expenses of the predictive value of the EKP Hamiltonian.

5 Calculation time

The calculation cycle to obtain the absorption coefficients in Figure 3 starts, according to the rule (a), for calculating envelope functions by solving the effective mass Schrödinger equation for the final state. Since, for the case of a box-shaped QD with squared potential, the solution is analytical and known beforehand, no time is needed for its determination. However the treatment used requires the numeric calculation of the eigenfunction in the nodes of the calculation lattice. This lattice, in our calculations, consists of 41×41×41 cells each of $1.5\times1.5\times1.5$ nm^3. The total number of nodes for calculation is 68,921. The time needed for this calculation is in the order of one second, using Mathematica 7 and a notebook (Core i5). For the EKPH this mesh has been verified to give similar results than double separation of mesh points and than double size cube sides, allowing for substantial time economy. After that, according to rule (b), the DFT must be calculated in a lattice of $\boldsymbol{k}$s. Subsequently, according to rule (c), it has to be multiplied by the proper element of the matrix in all the nodes of the $\boldsymbol{k}$-lattice (again 68,921). Finally, according to rule (d), the IDFT has to be obtained for all the elements of the *cb* row of the diagonalization matrix.

The same has to be done with the initial state, belonging to the *hh* or the *lh* bands. Once done, the matrix element of Eq. (9) is calculated through the numerical integration in the 68,921 nodes. For vertical illumination the matrix elements must be calculated for the *x* and *y* polarizations. Then they are introduced into the absorption coefficient of Eq. (7). The absorption coefficients of all the initial *hh* and *lh* states, which total about 200, are to be calculated in the same way and then they are interpolated and added to form each of VB→final state curves appearing in Figure 3. This takes about 8 min per curve. Since there are 12 curves this takes about 96 minutes. These operations and their calculation time are approximately the same for the EKP and the 4B Hamiltonians.

But for performing the aforementioned operations, the *cb*, *hh* and *lh* rows of the Hamiltonian diagonalization matrix have to have been calculated in the 68,921nodes of the $\boldsymbol{k}$-lattice. In total 12 matrix elements have to be calculated. In the EKP Hamiltonian, where the matrix elements are analytical, this takes less than one minute per element, that is, 12 min. In the 4B LKBP Hamiltonian the diagonalization process has to be undertaken for each $\boldsymbol{k}$-node. Consequently, it takes about 1.75 min per element; in total 21 min. Adding these values to the 96 min. of the preceding paragraph we obtain 108 min. for the EKP Hamiltonian and 117 min for the 4B LKPB Hamiltonian. This means that the calculation time of the 4B LKPB Hamiltonian is about 8% longer. We think that in practice the 4B LKPB Hamiltonian can be considered as fast as the EKP Hamiltonian. On the other hand, the calculation time for the 8B LKPB Hamiltonian has been estimated as 111 times more[16] than for the EKP Hamiltonian.

All the time calculations in this article are based on the use of Mathematica 7 and a notebook (Core i5), and the box shaped QDs with constant offset potentials. It is important to clarify that

calculation time may be reduced with more powerful software and machines, but this do not affect to the core of the paper: the use of a 4-band Hamiltonian reduces greatly the operation time.

6 Conclusions

The non-diagonal matrix blocs of the 8B LKPB Hamiltonian are made (0) to render the 8B-Hamiltonian of only 4 bands. The resulting Hamiltonian is adjusted so that the experimental *cb*, *hh* and *lh* effective masses and the strained QD bandgap are reproduced by changing some of the parameters used in the building of the Hamiltonian.

The nature of the crude field of strains necessary to obtain constant offsets in the the CB and VB edges, often considered, is stressed in this paper

The energy spectrum is calculated very quickly by using the multiband effective Schrödinger mass equations for a structure with box shaped QDs and constant energy offset. It is identical to that for the original 8B Hamiltonian and identical to that calculated with the EKP Hamiltonian, all resulting in the same effective mass equations. They all agree approximately with measurements of photoluminescence [33, 34] or photoreflectance [35] spectroscopy.

One element of the matrix $(D_{\boldsymbol{k}})_{i,j}$ that diagonalizes the Hamiltonian is used for the calculation of each envelope function; in total 12 elements calculate the envelope functions of the *cb*, *hh* and *lh* bands. Form a calculation time point of view the only difference with respect the EKP Hamiltonian is the calculation time of $(D_{\boldsymbol{k}})_{i,j}$, which in the EKP Hamiltonian is an analytic function whereas in the LKPB Hamiltonian it requires the Hamiltonian to be diagonalized in each $\boldsymbol{k}$-node of the calculation lattice. Nevertheless this involves only an average time increase of 8% in the calculation of each $(D_{\boldsymbol{k}})_{i,j}$.

The selection rules excluding transitions between states with different spins are clearly explained, as well as the similar nature of the (H_{uu}) and the (H_{ll}) matrices.

In summary, the calculation time of the absorption coefficients in the 4B LKPB Hamiltonian is only 8% longer than that of the EKP Hamiltonian, but it is about 100 times less than that with the 8B LKPB Hamiltonian.

IQE, calculated under the assumption of full collection as the current of the generated electron hole pairs, is rather close to the experimental one although that based in the EKP Hamiltonian seems slightly closer.

We consider that the 4B LKPB Hamiltonian fulfils the requirements for providing feedback to device scientists to develop better nanostructured solar cells.

Acknowledgments

This project has been supported by the Mega-grant 14B25.31.0020 from the Russian Ministry of Education and Science, the EC NGCPV (283798) grant and by the Spanish National Research Program PROMESA (ENE2012-37804-C02-01).

Appendix

The following auxiliary functions are used for the kinetic (LK) parts of the Hamiltonian

$$
\begin{aligned}
O_{LK} &= \gamma_c \frac{\hbar^2}{2m_0 q d^2}\left(K_x^2 + K_y^2 + K_z^2\right) \\
P_{LK} &= \gamma_1 \frac{\hbar^2}{2m_0 q d^2}\left(K_x^2 + K_y^2 + K_z^2\right) \\
Q_{LK} &= \gamma_2 \frac{\hbar^2}{2m_0 q d^2}\left(K_x^2 + K_y^2 - 2K_z^2\right) \\
R_{LK} &= \sqrt{3}\frac{\hbar^2}{2m_0 q d^2}\left[\gamma_2\left(K_x^2 + K_y^2\right) - 2i\gamma_3 K_x K_y\right] \\
S_{LK} &= \sqrt{6}\frac{\hbar^2}{2m_0 q d^2}\gamma_3 (K_x - iK_y) K_z \\
T_{LK} &= B(K_x + iK_y)/\sqrt{6} \\
U_{LK} &= BK_z/\sqrt{3}
\end{aligned}
\tag{A 1}
$$

In these equations the symbols m_0 and q are the mass and charge of the electron *in vacuo*; d is an arbitrary normalizing constant that here is taken as 1 nm. $\boldsymbol{K}$ is the wavevector normalized to $1/d$, that is, $\boldsymbol{K}=\boldsymbol{k}d$. The γs and B are parameters to be found in the Supplemental Supporting Material file.

With these functions the LK part of the block matrices is

$$
\left(H_{LK,uu}(\boldsymbol{K})\right) = \begin{pmatrix}
E_c + O_{LK} & -\sqrt{3}T_{LK} & \sqrt{2}U_{LK} & -U_{LK} \\
-\sqrt{3}T_{LK}^* & E_v - P_{LK} - Q_{LK} & \sqrt{2}S_{LK} & -S_{LK} \\
\sqrt{2}U_{LK}^* & \sqrt{2}S_{LK}^* & E_v - P_{LK} + Q_{LK} & -\sqrt{2}Q_{LK} \\
-U_{LK}^* & -S_{LK}^* & -\sqrt{2}Q_{LK}^* & E_v - P_{LK} - \Delta
\end{pmatrix}
\tag{A 2}
$$

and

$$
\left(H_{LK,ul}(\boldsymbol{K})\right) = \begin{pmatrix}
0 & 0 & -T_{LK}^* & -\sqrt{2}T_{LK} \\
0 & 0 & R_k & -\sqrt{2}R_k \\
T_{LK}^* & R_{LK} & 0 & \sqrt{3}S_{LK} \\
-U_{LK}^* & -S_{LK}^* & -\sqrt{3}S_{LK} & 0
\end{pmatrix}
\tag{A 3}
$$

The auxiliary functions for the strained (PB) parts of the Hamiltonian are,

$$
\begin{aligned}
O_{PB} &= a_c\left(\varepsilon_{xx}+\varepsilon_{yy}+\varepsilon_{zz}\right)\\
P_{PB} &= -a_v\left(\varepsilon_{xx}+\varepsilon_{yy}+\varepsilon_{zz}\right)\\
Q_{PB} &= -b_v\left(\varepsilon_{xx}+\varepsilon_{yy}+\varepsilon_{zz}\right)\\
R_{PB} &= -\frac{\sqrt{3}}{2}b_v(\varepsilon_{xx}-\varepsilon_{yy})+id_v\varepsilon_{xy}\\
S_{PB} &= -\frac{d_v}{\sqrt{2}}(\varepsilon_{zx}-i\varepsilon_{yz})\\
T_{PB} &= \frac{B}{\sqrt{6}}\left[(\varepsilon_{xx}+i\varepsilon_{yx})K_x+(\varepsilon_{xy}+i\varepsilon_{yy})K_y+(\varepsilon_{xz}+i\varepsilon_{yz})K_z\right]\\
U_{PB} &= \frac{B}{\sqrt{3}}K_z/\sqrt{3}(\varepsilon_{zx}K_x+\varepsilon_{zy}K_y+\varepsilon_{zz}K_z)
\end{aligned}
\tag{A 4}
$$

where the epsilons are the strain tensor elements.With these functions the PB part of the Hamiltonian is

$$
\left(H_{PB,uu}(\boldsymbol{K})\right)=\begin{pmatrix}
O_{PB} & -\sqrt{3}T_{PB} & \sqrt{2}U_{PB} & -U_{PB}\\
-\sqrt{3}T_{PB}^{*} & -P_{PB}-Q_{PB} & \sqrt{2}S_{PB} & -S_{PB}\\
\sqrt{2}U_{PB}^{*} & \sqrt{2}S_{PB}^{*} & -P_{PB}+Q_{PB} & -\sqrt{2}Q_{PB}\\
-U_{PB}^{*} & -S_{PB}^{*} & -\sqrt{2}Q_{PB}^{*} & -P_{PB}
\end{pmatrix}
\tag{A 5}
$$

The LKPB matrices for the strained material are obtained by adding to the LK matrices to the PB matrices. The remaining blocks are made up of the general relations, that is, $\left(H_{ll}(\boldsymbol{K})\right)=\left(H_{uu}^{*}(\boldsymbol{K})\right)$ and $\left(H_{lu}(\boldsymbol{K})\right)=\left(H_{ul}^{+}(\boldsymbol{K})\right)$.

References

[1] W. Shockley, H.J. Queisser, Detailed Balance Limit of Efficiency of p-n Junction Solar Cells, Journal of Applied Physics, 32 (1961) 510-519.

[2] A. Luque, A. Martí, Increasing the efficiency of ideal solar cells by photon induced transitions at intermediate levels, Physical Review Letters, 78 (1997) 5014–5017.

[3] A. Martí, L. Cuadra, A. Luque, Quantum dot intermediate band solar cell, in: Proc. 28th IEEE Photovoltaics Specialists Conference, IEEE, New York, 2000, pp. 940-943.

[4] C.G. Bailey, D.V. Forbes, S.J. Polly, Z.S.B. IEEE, Y. Dai, Chelsea Mackos, R.P. Raffaelle, S.M. Hubbard, Open-Circuit Voltage Improvement of InAs/GaAs Quantum-Dot Solar Cells Using Reduced InAs Coverage, IEEE Journal on Photovoltaics, (2012) DOI 10.1109/JPHOTOV.2012.2189047.

[5] V. Popescu, G. Bester, M.C. Hanna, A.G. Norman, A. Zunger, Theoretical and experimental examination of the intermediate-band concept for strain-balanced (In,Ga)As/Ga(As,P) quantum dot solar cells, Physical Review B, 78 (2008) 205321.

[6] S. Tomic, T.S. Jones, N.M. Harrison, Absorption characteristics of a quantum dot array induced intermediate band: Implications for solar cell design, Applied Physics Letters, 93 (2008) 263105.

[7] A. Luque, A. Marti, E. Antolín, P.G. Linares, I. Tobías, I. Ramiro, E. Hernandez, New Hamiltonian for a better understanding of the Quantum Dot Intermediate Band Solar Cells, Solar Energy Materials & Solar Cells, 95 (2011) 2095-2101.

[8] A. Luque, A. Mellor, Photon Absorption Models in Nanostructured Semiconductor Solar Cells and Devices, Springer, Cham, 2015.

[9] J.M. Luttinger, Quantum theory of cyclotron resonance in semiconductors - general theory, Physical Review, 102 (1956) 1030-1041.
[10] W. Kohn, Shallow impurity states in silicon and germanium, Solid State Physics-Advances in Research and Applications, 5 (1957) 257-320.
[11] G.E. Pikus, G.L. Bir, Effect of deformation on the energy spectrum and the electrical properties of imperfect germanium and silicon, Soviet Physics-Solid State, 1 (1959) 136-138.
[12] G.E. Pikus, G.L. Bir, Cyclotron and paramagnetic resonance in strained crystals, Physical Review Letters, 6 (1961) 103-105.
[13] G. Dresselhaus, A.F. Kip, C. Kittel, Plasma resonance in crystals - observations and theory, Physical Review, 100 (1955) 618-625.
[14] E.O. Kane, Energy band structure in p-type germanium and silicon, Journal of Physics and Chemistry of Solids, 1 (1956) 82-99.
[15] E.O. Kane, The k·p method, in: R.K. Willardson, A.C. Beer (Eds.) Physics of III-V Compounds, Academic, New York, 1966, pp. 75-100.
[16] A. Luque, A. Panchak, A. Mellor, A. Vlasov, A. Martí, V. Andreev, Comparing the Luttinger-Kohn-Pikus-Bir and the Empiric K.P Hamiltonians in quantum dot intermediate band solar cells manufactured in zincblende semiconductors Solar Energy Materials & Solar Cells, 141 (2015) 39-48.
[17] D. Bimberg, M. Grundmann, N.N. Ledentsov, Quantum Dot Hetrostructures, Wiley, 1999.
[18] C. Pryor, Eight-band calculations of strained InAs/GaAs quantum dots compared with one-, four-, and six-band approximations, Physical Review B, 57 (1998) 7190-7195.
[19] S. Tomic, A.G. Sunderland, I.J. Bush, Parallel multi-band k center dot p code for electronic structure of zinc blend semiconductor quantum dots, Journal of Materials Chemistry, 16 (2006) 1963-1972.
[20] A. Luque, A. Mellor, E. Antolin, P.G. Linares, I. Ramiro, I. Tobias, A. Marti, Symmetry considerations in the empirical k.p Hamiltonian for the study of intermediate band solar cells, Solar Energy Materials and Solar Cells, 103 (2012) 171-183.
[21] O.L. Lazarenkova, A.A. Balandin, Miniband formation in a quantum dot crystal, Journal of Applied Physics, 89 (2001) 5509-5515.
[22] M. Califano, P. Harrison, Approximate methods for the solution of quantum wires and dots: Connection rules between pyramidal, cuboidal, and cubic dots, Journal of Applied Physics, 86 (1999) 5054-5059.
[23] S. Datta, Quantum Phenomena, Addison Wesley, Reading (Mass), 1989.
[24] I. Vurgaftman, J.R. Meyer, L.R. Ram-Mohan, Band parameters for III-V compound semiconductors and their alloys, Journal of Applied Physics, 89 (2001) 5815-5875.
[25] K.W. Boer, Survey of Semiconductor Physics Van Nostrand Reinhold, New York, 1990.
[26] InAs: Effective Masses and Density of States, in, Ioffe Institute Data Basis.
[27] P.G. Linares, C.D. Farmer, E. Antolín, S. Chakrabarti, A.M. Sánchez, T. Ben, S.I. Molina, C.R. Stanley, A. Martí, A. Luque, Inx(GayAl1-y)1-xAs quaternary alloys for quantum dot intermediate band solar cells, Energy Procedia, 2 (2010) 133–141.
[28] E. Antolín, A. Marti, C.D. Farmer, P.G. Linares, E. Hernández, A.M. Sánchez, T. Ben, S.I. Molina, C.R. Stanley, A. Luque, Reducing carrier escape in the InAs/GaAs quantum dot intermediate band solar cell, Journal of Applied Physics, 108 (2010) 064513.
[29] V. Popescu, G. Bester, A. Zunger, Coexistence and coupling of zero-dimensional, two-dimensional, and continuum resonances in nanostructures, Physical Review B, 80 (2009) 045327.
[30] G. Bastard, Wave Mechanics Applied to Semiconductor Nanostructures, Les Editions de Physique, Paris, 1990.
[31] A. Luque, A. Marti, E. Antolin, P. Garcia-Linares, Intraband Absorption for Normal Illumination in Quantum Dot Intermediate Band Solar Cells, Solar Energy Materials & Solar Cells, 94 (2010) 2032–2035.

[32] A. Luque, A. Mellor, I. Tobías, E. Antolín, P.G. Linares, I. Ramiro, A. Martí, Virtual-bound, filamentary and layered states in a box-shaped quantum dot of square potential form the exact numerical solution of the effective mass Schrödinger equation, Physica B, 413 (2013) 73-81.
[33] S. Fafard, Z.R. Wasilewski, C.N. Allen, D. Picard, M. Spanner, J.P. McCaffrey, P.G. Piva, Manipulating the energy levels of semiconductor quantum dots, PHYSICAL REVIEW B, 59 (1999) 15368-15373.
[34] N.V. Kryzhanovskaya, A.G. Gladyshev, S.A. Blokhin, M.V. Maksimov, E. S. Semenova*, A.P. Vasil'ev, A.E. Zhukov, N.N. Ledentsov, V.M. Ustinov, D. Bimberg, Nonequilibrium Room-Temperature Carrier Distribution in InAs Quantum Dots Overgrown with Thin AlAs/InAlAs Layer, Semiconductors, 39 (2005) 1188-1193.
[35] E. Cánovas, A. Martí, N. López, E. Antolín, P.G. Linares, C.D. Farmer, C.R. Stanley, A. Luque, Application of the photoreflectance technique to the characterization of quantum dot intermediate band materials for solar cells, Thin Solid Films, 516 (2008) 6943–6947.

Graphical Abstract Caption

Sub-bandgap absorption calculated with the LKPB (H_{uu}) (thick black line) and contribution of the transitions from all the bound states in the *hh* and *lh* bands to the *cb* states (including the IB states). In the legends each curve is labeled with two letters for the initial states and the quantum numbers of the *cb* final state.

Highlights

- Four band Hamiltonian derived from ordinary 8 band LK-PB Hamiltonian
- Allows for two orders-of-magnitude faster calculations
- Reproduces reasonably well the quantum efficiency of a quantum dot solar cell
- Produces detailed absorption coefficient information
- Input for detailed balance analysis of nanostructured semiconductor devices